

Estimating Breakpoints between Climate States in Paleoclimate Data

Mikkel Bennedsen^{1,3}, Eric Hillebrand^{1,3}, Siem Jan Koopman², and Kathrine Larsen^{*1,3}

¹Department of Economics and Business Economics, Aarhus University, Denmark.

²Department of Econometrics, Vrije Universiteit Amsterdam, The Netherlands.

³Center for Research in Energy: Economics and Markets (CoRE), Aarhus University, Denmark.

August 14, 2024

This study presents a statistical time-domain approach for identifying transitions between climate states, referred to as breakpoints, using well-established econometric tools. We analyse a 67.1 million year record of the oxygen isotope ratio $\delta^{18}\text{O}$ derived from benthic foraminifera. The dataset is presented in Westerhold et al. (2020), where the authors use recurrence analysis to identify six climate states. Fixing the number of breakpoints to five, our procedure results in breakpoint estimates that closely align with those identified by Westerhold et al. (2020). By treating the number of breakpoints as a parameter to be estimated, we provide the statistical justification for more than five breakpoints in the time series. Further, our approach offers the advantage of constructing confidence intervals for the breakpoints, and it allows for testing how many breakpoints are present in the time series.

1 Introduction

Westerhold et al. (2020) present a time series dataset spanning from 67.1 million years ago (Ma) to the present time, covering the Cenozoic Era. Using recurrence analysis, the authors identify six different climate states in the data — Warmhouse I, Hothouse, Warmhouse II, Coolhouse I, Coolhouse II, and Icehouse. The climate states in the Cenozoic Era range from very warm climates to the glaciation of Earth’s polar regions (Zachos et al., 2001). The climatic transitions contain important information about variations in Earth’s climate system; see Tierney et al. (2020) for a review. Our study presents a statistical approach for identifying the transitions between climate

* Authors are listed in alphabetical order. Corresponding author: kblarsen@econ.au.dk

states, referred to as *breakpoints*, using econometric time-domain tools proposed by Bai and Perron (1998, 2003). This approach offers the advantages of constructing confidence intervals for the dates of the breakpoints, providing a measure of estimation uncertainty, as well as testing for the number of breakpoints in the time series.

The methodology used by Westerhold et al. (2020) to identify breakpoints is recurrence analysis, as described by Marwan et al. (2007). To conduct this analysis, Westerhold et al. (2020) resampled their data at a frequency of 5 thousand years (kyr) and used both un-detrended and detrended versions of the data. This analysis leads to the identification of the six climate states.

The use of recurrence analysis to identify climate states is common in the study of paleoclimate time series, see the review in Marwan et al. (2021). Many extensions to this methodology have been made to address different issues. Goswami et al. (2018) propose a breakpoint detection method using a probability density function sequence representation of the time series, which allows for uncertainties in the time stamping of the time series. Bagniewski et al. (2021) combine recurrence analysis with Kolmogorov–Smirnov tests to detect abrupt transitions in a time series. Rousseau et al. (2023) applies this method on the Westerhold et al. (2020) data and find similar climate states as the ones reported in Westerhold et al. (2020). As discussed by Marwan et al. (2021), there are several other approaches to identify transitions in paleoclimate time series. Among these, Livina et al. (2010) developed a statistical method to detect the number of states in a time series using potential analysis.

Our approach contributes to the existing breakpoint detection methods in paleoclimate research by applying well-established econometric tools in the time-domain, developed in Bai and Perron (1998, 2003), to identify climate states in the paleo record. It enables the estimation of multiple breakpoints along with confidence intervals and provides procedures to estimate the number of breakpoints.

The estimation methodology of Bai and Perron (1998, 2003) necessitates a constant observation frequency and a predetermined model specification. To obtain a constant observation frequency, we use mean binning, which entails dividing the data into intervals of fixed length and calculating the mean in each bin. We explore three different model specifications and implement these using the R-package by Nguyen et al. (2023). The first model is a state-dependent mean model, which is equivalent to a model with an abrupt break in the mean of $\delta^{18}\text{O}$ for each climate state. The second model generalises this by including a state-independent autoregressive term, which can be interpreted as making the transitions between states more gradual. The final model extends the second model by letting the autoregressive term be state-dependent as well, allowing for state-specific transition dynamics. All models incorporate an error term with state-dependent variance. Given

that the time series appears state-wise non-stationary, meaning that the mean and/or the variance of the time series vary over time within a state, we conduct a simulation study to demonstrate the applicability of the approach by Bai and Perron (1998, 2003) in this non-stationary setting.

The number of breakpoints is a parameter in the statistical approach of Bai and Perron (1998, 2003). Fixing the number of breakpoints to five, the resulting breakpoint estimates align closely with those identified by Westerhold et al. (2020) across various binning frequencies and model specifications. This demonstrates the robustness of the approach and corroborates the dating of the climate states of Westerhold et al. (2020) with statistical analysis in the time domain. However, when we allow the number of breakpoints to vary and treat this as a parameter to be estimated using information criteria, we find strong statistical evidence for the presence of more than five breakpoints. Specifically, our analysis suggests that Warmhouse II and Coolhouse II can each be split into two separate substates.

The remainder of the paper is structured as follows: In Section 2, we present the $\delta^{18}\text{O}$ dataset and climate states by Westerhold et al. (2020). In Section 3, the statistical breakpoint detection methodology applied in this paper is outlined. In Section 4, we conduct the analysis and discuss the results. Section 5 concludes. The finite sample performance of the methodology under state-wise non-stationarity is investigated in a simulation study in Appendix A.

2 Data

The paleoclimate variable $\delta^{18}\text{O}$ measures the ratio of ^{18}O to ^{16}O in the shells of benthic foraminifera obtained from ocean sediment cores, relative to a standard sample. The weight difference between the oxygen isotopes leads to an inverse relationship between $\delta^{18}\text{O}$ and ocean temperatures; see for instance Epstein et al. (1951) and Shackleton (1967).

In this paper, we use the dataset provided in the study by Westerhold et al. (2020) which compiles measurements of oxygen and carbon isotope ratios from benthic foraminifera across 34 different studies and 14 ocean drilling locations into a single data file. Our study focuses on the $\delta^{18}\text{O}$ record, specifically the correlation-corrected observations of $\delta^{18}\text{O}$ (column “benthic d18O VPDB Corr” from the data file). Westerhold et al. (2020) provide an estimated chronology of the data, which has accuracy ranging from ± 100 kyr in the older part of the sample period to ± 10 kyr in the younger part. We ignore the uncertainty of the time stamps in this study. The data cover the period 67.10113 Ma to 0.000564 Ma, and we order the observations from oldest to most recent. We remove the 74 missing values in the record, leaving us with 24,259 data points.

The six climate states identified by Westerhold et al. (2020) are Warmhouse I (66-56 Ma), Hothouse (56-47 Ma), Warmhouse II (47-34 Ma), Coolhouse I (34-13.9 Ma), Coolhouse II (13.9-

3.3 Ma), and Icehouse (3.3 Ma to present). The top panel of Figure 1 shows the $\delta^{18}\text{O}$ data with the breakpoints between the climate states as identified by Westerhold et al. (2020). Summary statistics of the dataset for the full sample length and for each climate state are presented in Appendix C.1.

The $\delta^{18}\text{O}$ data presents unique challenges due to its irregular nature and intermittent gaps. The bottom panel of Figure 1 shows the time series of increments between consecutive time stamps in the record. This shows that the time series is relatively sparse in the older part of the record and relatively dense in the younger part. The average time between two adjacent data points is approximately 2.8 kyr, and the longest gap between data points is approximately 115.4 kyr. There are 533 occurrences of gaps between two data points lasting longer than 10 kyr. Moreover, there are 591 instances of multiple observations at the same time stamp, with up to four simultaneous observations.

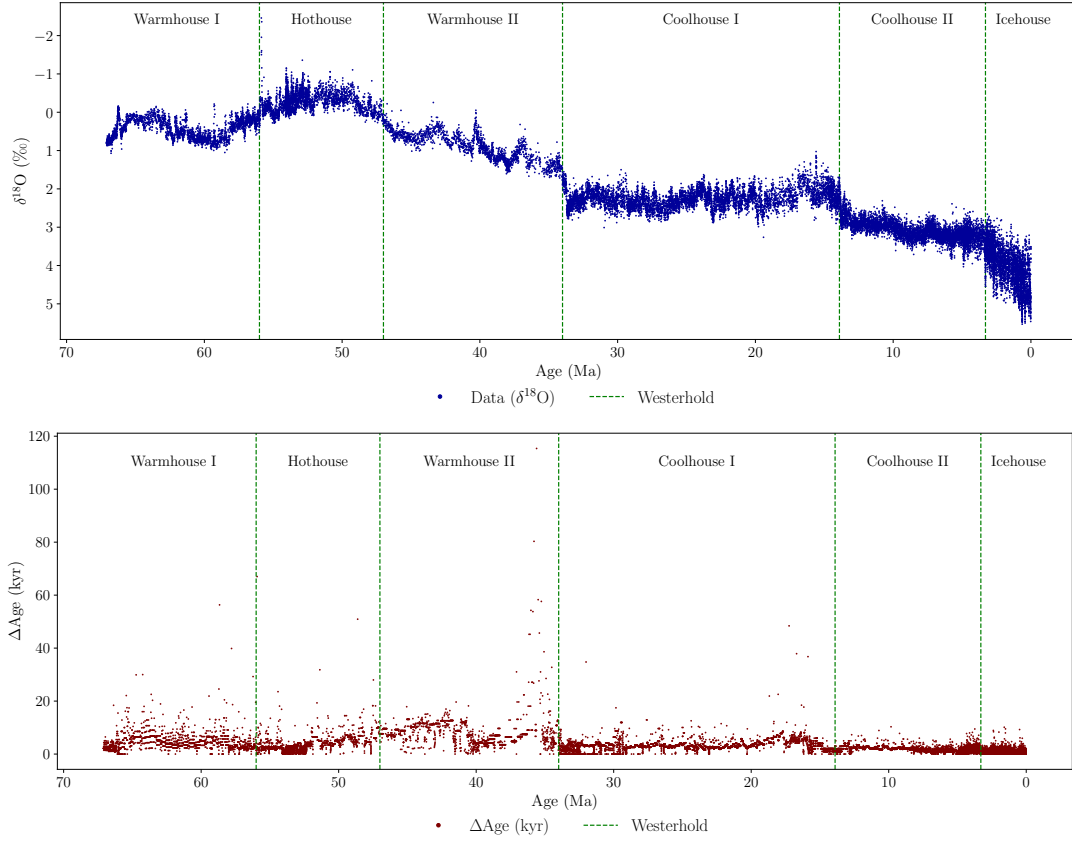


Figure 1: Top panel: $\delta^{18}\text{O}$ data from Westerhold et al. (2020). Bottom panel: The time between data points of $\delta^{18}\text{O}$ data measured in kyr. The vertical dashed lines denoting transitions between the climate states by Westerhold et al. (2020). The horizontal axis represents time, measured in millions of years before present.

3 Methodology

In this section, we present and discuss the methodology developed by Bai and Perron (1998, 2003) for estimating breakpoints in linear regression models. Section 3.1 provides an outline of the framework for detecting multiple structural changes in linear regression coefficients. Section 3.2 discusses the model specifications employed in this study for breakpoint estimation. Section 3.3 outlines the implementation of the model specifications.

3.1 General framework

The method is based on minimising the sum of squared residuals while treating the breakpoints as unknown parameters to be estimated (Bai and Perron, 1998, 2003). Consider a linear regression framework for the dependent variable y_t , for $t = 1, \dots, T$, and with m breakpoints, corresponding to $m + 1$ distinct states in the sample, and with model equation

$$y_t = x_t' \beta + z_t' \delta_j + u_t, \quad t = T_{j-1} + 1, \dots, T_j, \quad (1)$$

with $j = 1, \dots, m + 1$. The m break dates are denoted by (T_1, \dots, T_m) with the convention that $T_0 = 0$ and $T_{m+1} = T$ and u_t is the disturbance term with mean zero and variance σ_j . The $(p \times 1)$ -vector x_t and the $(q \times 1)$ -vector z_t comprise two sets of covariate vectors, for which β is the state-independent vector of coefficients and δ_j is the state-dependent vector of coefficients. Since only specific coefficients are subject to structural breaks, this model is referred to as a partial structural change model. Moreover, breaks in the variance of u_t at the break dates T_1, \dots, T_m can be considered, such that $\sigma_i \neq \sigma_j$ for $i \neq j$. The parameters β and δ_j are estimated alongside the breakpoints but are not of primary interest here.

We will treat the number of breakpoints, m , as known for now and estimate the coefficients and the breakpoints using a sample of T observations of $\{y_t, x_t, z_t\}$. The estimation method is based on least squares for both the coefficients and the breakpoints. For each possible set of m breakpoints (T_1, \dots, T_m) denoted as $\{T_i\}_{i=1}^m$, we obtain estimates of β and δ_j by minimising the sum of squared residuals (SSR), that is,

$$SSR = \sum_{j=1}^{m+1} \sum_{t=T_{j-1}+1}^{T_j} (y_t - x_t' \beta - z_t' \delta_j)^2, \quad (2)$$

where β is common to all states, while δ_j is specific for the state j , which is the period between $T_{j-1} + 1$ and T_j . The resulting estimated coefficients are denoted as $\hat{\beta}(\{T_i\}_{i=1}^m)$ and $\hat{\delta}(\{T_i\}_{i=1}^m)$. These coefficients are then used to determine the SSR associated with each set of breakpoints,

$$SSR_T(\{T_i\}_{i=1}^m) \equiv \sum_{j=1}^{m+1} \sum_{t=T_{j-1}+1}^{T_j} \left(y_t - x_t' \hat{\beta}(\{T_i\}_{i=1}^m) - z_t' \hat{\delta}(\{T_i\}_{i=1}^m) \right)^2. \quad (3)$$

The estimated breakpoints are then given by

$$\left(\hat{T}_1, \dots, \hat{T}_m\right) = \underset{T_1, \dots, T_m}{\operatorname{argmin}} \text{SSR}_T(\{T_i\}_{i=1}^m). \quad (4)$$

The minimisation is conducted over all partitions (T_1, \dots, T_m) such that $T_j - T_{j-1} \geq \dim(z_t)$ to ensure that there are enough data points to estimate the parameters δ_j in each partition. This procedure leads to estimated parameters for the m breakpoints, i.e., $\left\{\hat{T}_i\right\}_{i=1}^m$, $\hat{\beta} = \hat{\beta}\left(\left\{\hat{T}_i\right\}_{i=1}^m\right)$, and $\hat{\delta} = \hat{\delta}\left(\left\{\hat{T}_i\right\}_{i=1}^m\right)$. Since the breakpoints are discrete, this optimisation can be conducted using a grid search, which can be computationally heavy, especially for many breakpoints. Bai and Perron (2003) introduce an efficient method for determining the global minimisers.

An essential advantage of this framework is that it allows for constructing confidence intervals for the breakpoints, something that is not available for the recurrence analysis approach implemented in Westerhold et al. (2020). The construction of confidence intervals is based on the asymptotic distribution of the break dates. The convergence results for the construction of confidence intervals rely on a number of assumptions (see Bai and Perron, 2003), which may possibly be violated for the $\delta^{18}\text{O}$ data. To examine whether the framework is adequate for the type of data studied here, we conducted a large simulation study, the details of which are reported in Appendix A. We discuss the results from the simulation study, and how they relate to the analysis of the $\delta^{18}\text{O}$ data, below.

3.2 Model specifications

In this section, we introduce the model specifications employed in this paper for estimating breakpoints. Three distinct specifications are considered, referred to as the "Mean", "Fixed AR", and "AR" models, where AR refers to the autoregressive model of order one with intercept. These are all special cases of the framework outlined in Equation (1). The simplest among them, the Mean model, is specified as follows,

$$y_t = c_j + u_t, \quad t = T_{j-1} + 1, \dots, T_j, \quad (5)$$

where $j = 1, \dots, m + 1$. In this model, c_j is the state-dependent intercept and u_t is an error term. This model is equivalent to setting $x_t = 0$, $z_t = 1$, and $\delta_j = c_j$ in Equation (1). A breakpoint in this model specification leads to an abrupt change in the mean of the dependent variable y_t .

The Fixed AR model extends the Mean model by incorporating an autoregressive term. We obtain the model

$$y_t = c_j + \varphi y_{t-1} + u_t, \quad t = T_{j-1} + 1, \dots, T_j, \quad (6)$$

and $j = 1, \dots, m + 1$. Here, y_{t-1} is the dependent variable lagged by one period, and φ is the autoregressive coefficient that is constant over the whole sample. In this model, the effect of a

change in the coefficient c_j is more gradual since it depends on the autoregressive dynamics. The Fixed AR model is obtained from Equation (1) by specifying $x_t = y_{t-1}$, $\beta = \varphi$, $z_t = 1$, and $\delta_j = c_j$.

The general AR specification also allows the autoregressive term to be state-dependent, resulting in the AR model,

$$y_t = c_j + \varphi_j y_{t-1} + u_t, \quad t = T_{j-1} + 1, \dots, T_j, \quad (7)$$

where $j = 1, \dots, m+1$ and the autoregressive coefficient φ in Equation (6) is now state-dependent, denoted φ_j . This model is obtained from Equation (1) by setting $x_t = 0$, $z_t = (1, y_{t-1})$, and $\delta_j = (c_j, \varphi_j)$. Here, both the intercept and the autoregressive coefficient are state-dependent. Thus, the three specifications are nested: The AR model is the most general; the Fixed AR model is nested in the AR model by setting $\varphi_1 = \varphi_2 = \dots = \varphi_{m+1}$, and the Mean model is nested in the Fixed AR model by setting $\varphi = 0$.

3.3 Implementation

The models are implemented using the *mbreaks* R-package (Nguyen et al., 2023) based on the methodology of Bai and Perron (1998, 2003). For all model specifications, we set the minimum length of a state, h , to 2.5 million years (Myr), facilitating the estimation of shorter climate states. Also, we let the variance of the error term, denoted as σ_j^2 , be state-dependent.

As outlined by Bai and Perron (2003), no serial correlation is permitted in the errors of the regressions. However, the time series of $\delta^{18}\text{O}$ is likely subject to both autocorrelation and heteroscedasticity. The assumption of no serial correlation in the errors may be violated in the model specifications considered in this paper, since the incorporation of only up to one lag in the covariates is unlikely to remove serial correlation in the errors.

To address these issues, we use the autocorrelation and heteroscedasticity consistent (HAC) covariance matrix estimator with prewhitening in our implementations. The prewhitening procedure, proposed by Andrews and Monahan (1992), entails applying an autoregressive model with one lag to $z_t \hat{u}_t$, where \hat{u}_t denotes the residuals. The HAC covariance matrix estimator by Andrews (1991) is then constructed based on the filtered series using the quadratic spectral kernel with bandwidth selected by an AR of order one approximation. This approach is used for both the Mean, Fixed AR, and AR models.

4 Analysis and results

This section presents the results of the breakpoint analysis of the $\delta^{18}\text{O}$ record. The irregular sampling is addressed by data binning in Section 4.1, where the stationarity properties of binned

data are assessed. In Section 4.2, we fix the number of breakpoints to five as in Westerhold et al. (2020). In Section 4.3, we treat the number of breakpoints as a parameter to be estimated.

4.1 Constant data frequency

To conduct breakpoint estimation using the methodology of Bai and Perron (1998, 2003), we need an equidistant time series. We use a binning approach to construct a dataset with evenly-spaced observations, which is common practice in the analysis of paleoclimate data; see for instance Boettner et al. (2021) or Reikard (2021). We divide the dataset into bins of fixed time intervals and compute the mean of the observations within each bin. In the case of gaps in the binned data, we use the values immediately preceding and succeeding the section with missing data to perform linear interpolation. We consider six different bin sizes, namely 5, 10, 25, 50, 75, and 100 kyr. Summary statistics for the full sample length and for each climate state identified by Westerhold et al. (2020) for all binning frequencies are provided in Appendix C.1. Figure 2 shows the binning approach, with the top panel showing unaltered data and binned data at 5 kyr and 100 kyr frequencies, and the bottom panels zooming in on two sub-samples.

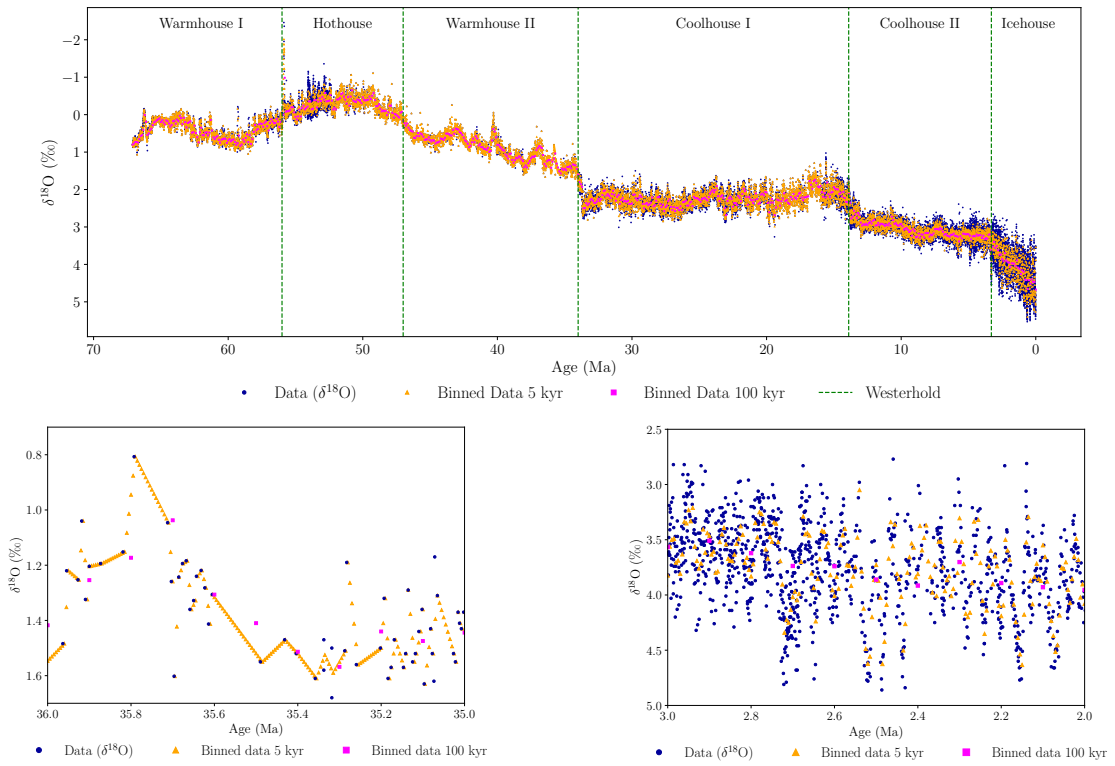


Figure 2: Top panel: The original data and the 5 and 100 kyr binned data. Bottom left panel: The period 36-35 Ma. Bottom right panel: The period 3-2 Ma.

The top panel of Figure 2 shows that data binned at higher frequencies follow the variations in the dataset more closely, whereas data binned at lower frequencies tend to be smoother. Notably,

the longest gap in the dataset spans approximately 115 kyr and occurs between 36 Ma and 35 Ma. The bottom panels in Figure 2 zoom in on the periods 36 to 35 Ma (left) and 3 to 2 Ma (right). These plots illustrate that in case of large gaps (left), a high binning frequency results in linear interpolation between observations. This effect does not occur for periods with many observations (right), where low binning frequencies capture only a small part of the variation in the original data. Binning offers a simple approach to handle the uneven frequency of the dataset. However, it leads to data loss at lower binning frequencies and to the introduction of artificial data points resulting from linear interpolation at higher binning frequencies. The selection of binning frequencies can therefore alter the properties of the time series, potentially misrepresenting the dynamics of the original data. In another paper Bennedsen et al. (2024), we propose a continuous-time state-space framework to analyze the entire time series without data aggregation.

4.1.1 Stationarity of the binned data

The theoretical framework by Bai and Perron (1998, 2003) is developed for estimating and testing for multiple breakpoints in linear regression models where the regressors are non-trending or state-wise stationary. However, the $\delta^{18}\text{O}$ data appears state-wise non-stationary over most of the record. As pointed out by Kejriwal et al. (2013), if the time series maintains its stationarity properties over the respective states, the methods developed for stationary data are still applicable for these cases. However, if the process alternates between stationary and non-stationary states, the theoretical properties of the methodology are unknown.

To investigate whether the time series is non-stationary, we apply the Augmented Dickey-Fuller (ADF) test (Dickey and Fuller, 1979), with the null hypothesis of non-stationarity. For the entire 25 kyr binned data sample, the ADF test does not reject the null hypothesis at the 1% significance level, indicating non-stationarity. However, when examining the binned data for each climate state identified by Westerhold et al. (2020) separately, the ADF test rejects the null hypothesis at the 1% significance level for the Warmhouse II, Coolhouse I, and Icehouse states. These tests indicate the presence of state-wise non-stationarity, and we therefore need to examine whether the methodology of Bai and Perron (1998, 2003) is applicable to data-generating processes that are state-wise non-stationary or alternating between stationary and non-stationary states.

We conduct a simulation study to examine potential challenges in conducting breakpoint estimation on these types of data-generating processes using the three model specifications. The study is conducted for both independent and identically distributed (i.i.d.) error terms and serially correlated error terms in Appendices A.1 and A.2, respectively. The results show that the procedure works well with non-stationarity and is robust to processes with one stationary and one

non-stationary state for Fixed AR and AR models. However, the Mean model performs poorly with highly persistent data-generating processes. In the case of serial correlation, the results are less conclusive, but if the states are sufficiently different, the methodology still appears effective. The study also reveals that the coverage rates of the estimated confidence intervals are generally adequate for the Fixed AR model specification in cases of large breaks. In contrast, the confidence intervals for the AR model are too narrow in many of the data-generating processes considered.

4.2 Fixing the number of breakpoints to five

In this section, we fix the number of five breakpoints as reported in Westerhold et al. (2020). We estimate the breakpoints and corresponding 95% confidence intervals for each of the binning frequencies, 5, 10, 25, 50, 75, and 100 kyr. In each estimation, we use a minimum state length of 2.5 Myr, allowing us to estimate relatively short climate states. The estimation results are tabulated in Appendix C.2 and are shown in Figure 3, with subfigures for the Mean, Fixed AR, and AR models. The estimated confidence intervals around the breakpoints are often asymmetrical. Bai and Perron (2003) advocate the use of asymmetric confidence intervals, as these provide better coverage rates when the data are non-stationary.

For the Mean model in Figure 3a, it is evident that the estimated breakpoints generally remain at the same dates throughout as the binned data frequency decreases step-by-step from 5 kyr to 100 kyr. The width of the 95% confidence intervals increases as the frequency decreases, which can be attributed to the resultant decrease in the number of binned observations available for estimation at the lower frequencies. All the breakpoints align with those identified by Westerhold et al. (2020). A similar pattern of alignment is observed in the Fixed AR model, albeit with tighter confidence intervals, as depicted in Figure 3b.

Figure 3c presents the findings for the AR model, which exhibits more sensitivity to the frequency of the binned data. At higher frequencies, the breakpoints tend to appear in the more recent parts of the sample. However, as the frequency decreases further, the breakpoints are estimated to be in the older parts of the sample period. For the results using 25 kyr, we find that the estimated breakpoints from the three model specifications align closely. The estimated breakpoints align almost perfectly with those identified by Westerhold et al. (2020) and hence strongly corroborate their findings.

As a robustness check, we re-estimate the model specifications for five breakpoints using the 25 kyr binned data reversed with respect to the time dimension, i.e., letting time run backwards. The results are shown in Appendix B.1. We find that the results of the Mean and Fixed AR models are robust to reversing the time frame, with almost unchanged estimated breakpoints. Conversely,

the AR model leads to estimated breakpoints in the more recent part of the sample, resulting in breakpoints at 16.9 Ma and 9.7 Ma, which differ from those estimated using the same model and binning frequency with time running forward.

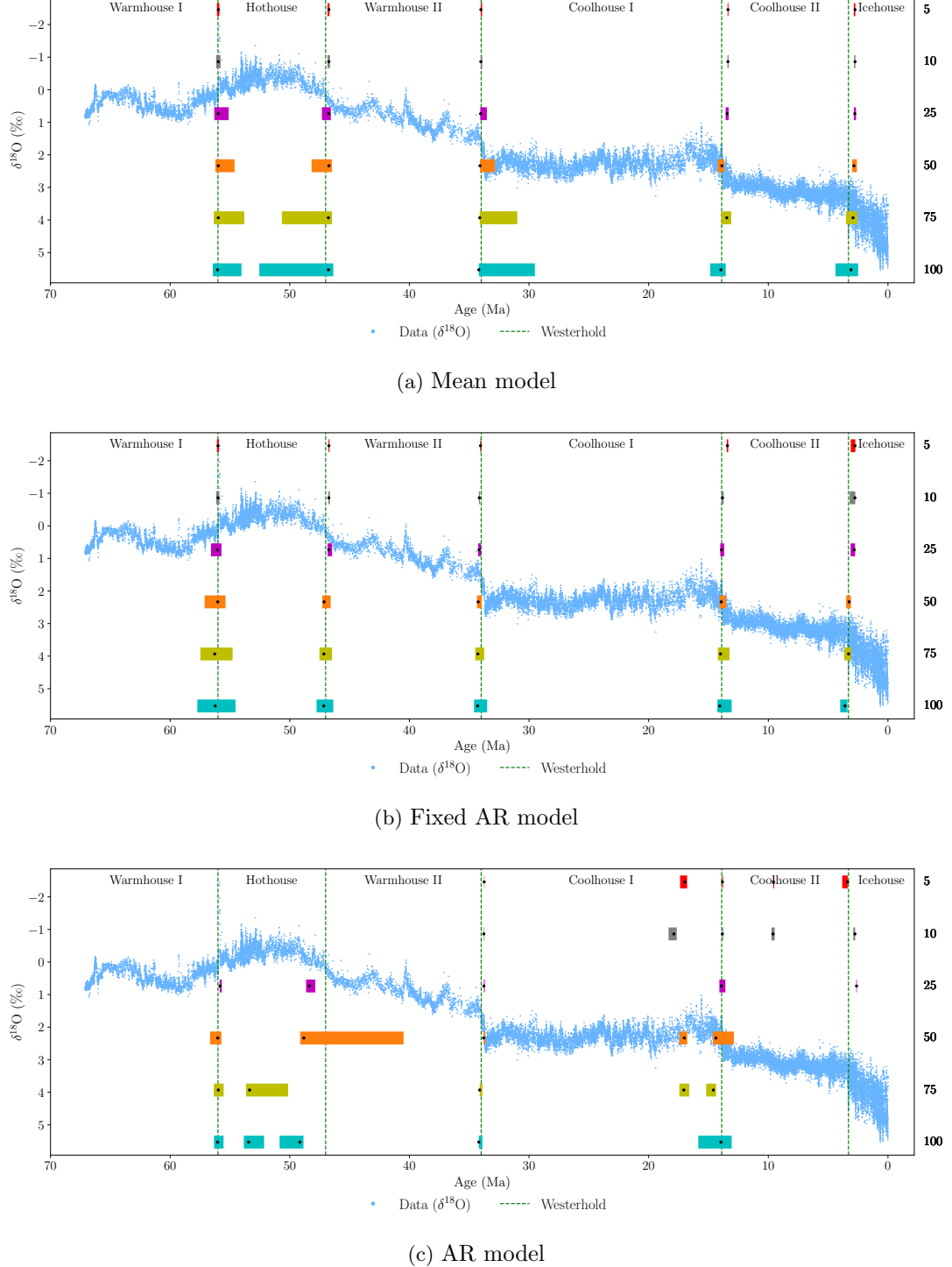


Figure 3: A comparison of estimated breakpoints using binned data with frequencies of 5, 10, 25, 50, 75, and 100 kyr from top to bottom, fixing the number of breakpoints to five for each model specification. The black dots represent estimated breakpoints, while coloured shaded rectangles indicate 95% confidence intervals. The results overlay the $\delta^{18}\text{O}$ data from Westerhold et al. (2020) and their climate states.

To summarise, the results of the Mean and Fixed AR models exhibit robustness across different binning frequencies, whereas the AR model appears more sensitive to variations in binning frequency and the reversal of the time dimension. As detailed in the simulation study in Appendix A, the Mean model fails to accurately detect breakpoints in highly persistent data-generating processes. Consequently, in what follows, we focus on the Fixed AR model for the estimation of breakpoints in the $\delta^{18}\text{O}$ time series. Furthermore, we recommend using binning frequencies 10 and 25 kyr as they result in the most consistent outcomes.

4.3 Estimating the number of breakpoints

We use information criteria to estimate the number of breakpoints. We initially consider the following three criteria: the Bayesian Information Criterion (BIC) by Yao (1988), the modified Schwarz Information Criterion (LWZ) by Liu et al. (1997), and the modified BIC (KT) by Kurozumi and Tuvaandorj (2011). For all criteria, the estimated number of breakpoints is determined as the number of breakpoints that minimises the information criterion in question.

Bai and Perron (2006) note that the BIC and LWZ criteria perform well in absence of serial correlation, but both of them lead to overestimation of the number of breakpoints in case of serial correlation in the error term. In simulation studies, reported in Appendices A.1 and A.2, we find that the KT information criterion performs poorly, and hence, we exclude it from the subsequent analysis. We also find that the number of breakpoints estimated using the Mean model specification is generally overestimated when employing the information criteria. For the Fixed AR and AR models, the BIC and LWZ criteria typically perform well, especially in data-generating processes with a large break. With serial correlation in the error term, the BIC criterion tends to overestimate the number of breakpoints, whereas the LWZ criterion generally performs well in the Fixed AR and AR model specifications.

We use the BIC and LWZ information criteria for each model specification and binning frequency, and set the minimum state length to $h = 2.5$ Myr. Table 1 shows the estimated number of breakpoints. There is a tendency towards higher numbers with increasing binning frequency, and for the BIC to indicate higher numbers than the LWZ criterion. For our preferred specification, the Fixed AR model with 25 kyr binning frequency, the LWZ and BIC criteria suggests 6 and 12 breakpoints, respectively. For a 10 kyr binning frequency, the estimated number of breakpoints are 7 and 14, respectively. Thus, the information criteria indicate that the number of distinct climate states in the $\delta^{18}\text{O}$ record is larger than the five suggested in Westerhold et al. (2020).

To further investigate a higher number of breakpoints, we consider the estimation of up to fifteen breakpoints. As previously discussed, we advocate for using the Fixed AR model and mid-range

binning frequency. Therefore, we estimate one to fifteen breakpoints using the Fixed AR model and 25 kyr binned data. The results are shown in Figure 4. When five or more breakpoints are allowed for, we find that the five breakpoints identified by Westerhold et al. (2020) consistently coincide with five of the estimated breakpoints using our approach, indicating the robustness of these five breakpoints. Allowing for six breakpoints, we get an additional breakpoint in Warmhouse II that remain for higher numbers. Allowing for seven, we get another one in Coolhouse II; allowing for eight, another in Icehouse; allowing for nine another in Coolhouse I; and so on.

Additionally, the estimation results justify dividing the climate states Warmhouse II and Coolhouse II into two substates each at approximately 39.7 Ma and 10 Ma, respectively. This is supported by the presence of breakpoints estimated approximately at these time stamps in the estimations with seven or more breakpoints. Comparable findings are presented in Appendices B.2 and B.3, which detail the results of estimating one to fifteen breakpoints using the Mean and AR models, respectively, with 25 kyr binned data.

Bin size	Mean		Fixed AR		AR	
	BIC	LWZ	BIC	LWZ	BIC	LWZ
5	19	17	17	7	15	5
10	17	17	14	7	14	3
25	17	14	12	6	8	3
50	17	14	10	0	7	0
75	17	14	6	0	5	0
100	17	12	6	0	5	0

Table 1: The number of breakpoints estimated using BIC and LWZ criterion for all models and binning frequencies considered. The minimum state length is set to $h = 2.5$ Myr and the maximum number of breakpoints is 26.

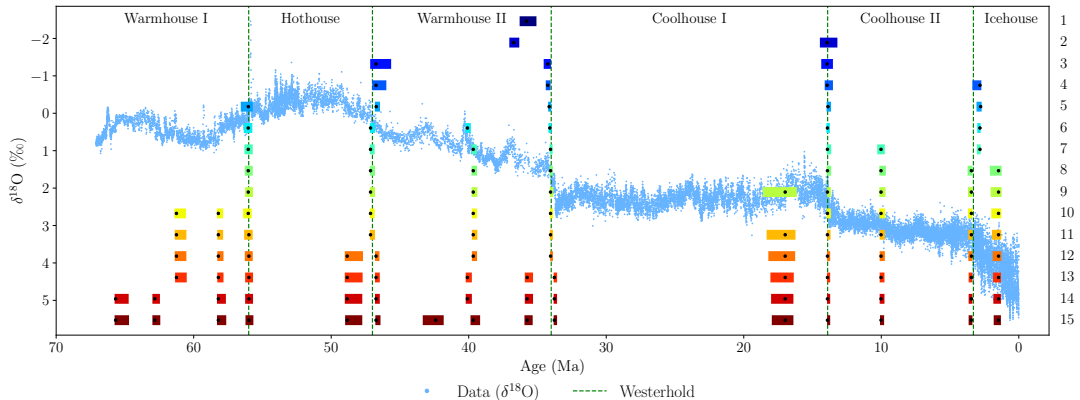


Figure 4: A comparison of estimated breakpoints using the Fixed AR model for one to fifteen breakpoints on 25 kyr binned data. The minimum state length is set to $h = 1$ Myr. The black dots represent estimated breakpoints, while coloured shaded rectangles indicate 95% confidence intervals. The results overlay the $\delta^{18}\text{O}$ data from Westerhold et al. (2020) and their climate states.

5 Conclusion

In this study, we propose a statistical approach to the estimation of breakpoints between climate states in the Cenozoic Era. We analyse the 67.1 million-year record of $\delta^{18}\text{O}$ presented by Westerhold et al. (2020). The authors of the study use recurrence analysis to identify five breakpoints, thus defining six climate states. We employ the well-established econometric time-domain tools developed by Bai and Perron (1998, 2003). Within this framework, we consider three model specifications: a state-dependent mean model, an extended version with a state-independent autoregressive (AR) term, and a further extension with a state-dependent AR term. All models incorporate an error term with state-dependent variances. The first model corresponds to modelling an abrupt break in the mean of $\delta^{18}\text{O}$. The state-independent AR term in the second model allows for more gradual transitions between states. The final model introduces fully state-dependent autoregressive dynamics. Our approach allows for the construction of confidence intervals for the breakpoints, thereby providing a measure of estimation uncertainty. Furthermore, it allows for testing for the number of breakpoints in the time series.

The binned $\delta^{18}\text{O}$ data exhibit non-stationarity, also within climate states. In a simulation study, we demonstrate that the methodology of Bai and Perron (1998, 2003) is applicable in time series exhibiting state-wise non-stationarity and switching between stationarity and non-stationarity, even when incorporating serial correlation in the error term. Our examination of information criteria for estimating the number of breakpoints shows varying effectiveness across models in the simulation study. However, the model specification with a state-independent AR term shows promising results in both accuracy of breakpoint estimation and coverage rates of confidence intervals. Moreover, using the BIC and LWZ criterion in this model specification leads to high accuracy in estimating the number of breakpoints.

The estimation of the models requires evenly time-stamped data, and therefore, we apply mean binning. We consider multiple binning frequencies: 5, 10, 25, 50, 75, and 100 kyr. To maintain comparability with the findings of Westerhold et al. (2020), we fix the number of breakpoints to five. This results in breakpoint estimates closely aligning with those identified by Westerhold et al. (2020) across various binning frequencies and the model specifications, demonstrating the robustness of the approach. These results corroborate the dating of the transitions between climate states of Westerhold et al. (2020) with time series analysis.

Then, we treat the number of breakpoints as a parameter to be estimated using information criteria. The results vary depending on the model specification and the binning frequency. Based on the results of our simulation study, we advocate the using the model specification with a state-independent AR term. Furthermore, we recommend a binning frequency in the mid-range, which

generally capture the dynamics of the original data most accurately. Then, we find statistical evidence for more than five breakpoints in the time series. Specifically, we find evidence that Warmhouse II and Coolhouse II can be split into two substates each. The two splits along with the five breakpoints also found by Westerhold et al. (2020) are also preserved when considering more than seven breakpoints.

There are many directions in which our work could be extended in the future, given the unresolved issues in the statistical analysis of paleoclimate time series. These include, but are not limited to, unevenly time-stamped data, multiple observations at the same time stamp, and measurement errors. In a follow-up project outlined in Bennedsen et al. (2024), we propose a continuous-time state-space framework for analysing the time series data by Westerhold et al. (2020), taking their breakpoints as given. This framework allows us to address the issues mentioned. Regarding breakpoint detection, it is evident that the binning method used in this study results in a considerable loss of information. Future research will aim to address this issue.

References

Andrews, D. W. K. (1991). Heteroskedasticity and Autocorrelation Consistent Covariance Matrix Estimation. *Econometrica*, 59(3):817–858.

Andrews, D. W. K. and Monahan, J. C. (1992). An Improved Heteroskedasticity and Autocorrelation Consistent Covariance Matrix Estimator. *Econometrica*, 60(4):953–966.

Bagniewski, W., Ghil, M., and Rousseau, D. D. (2021). Automatic detection of abrupt transitions in paleoclimate records. *Chaos*, 31(11):113129.

Bai, J. and Perron, P. (1998). Estimating and Testing Linear Models with Multiple Structural Changes. *Econometrica*, 66(1):47–78.

Bai, J. and Perron, P. (2003). Computation and analysis of multiple structural change models. *Journal of Applied Econometrics*, 18(1):1–22.

Bai, J. and Perron, P. (2006). *Multiple Structural Change Models: A Simulation Analysis*, page 212–238. Cambridge University Press.

Bennedsen, M., Hillebrand, E., Koopman, S. J., and Larsen, K. B. (2024). Continuous-time state-space methods for delta-O-18 and delta-C-13. arXiv:2404.05401.

Boettner, C., Klinghammer, G., Boers, N., Westerhold, T., and Marwan, N. (2021). Early-warning signals for Cenozoic climate transitions. *Quaternary Science Reviews*, 270:107177.

Dickey, D. and Fuller, W. (1979). Distribution of the Estimators for Autoregressive Time Series With a Unit Root. *Journal of the American Statistical Association*, 74.

Epstein, S., Buchsbaum, R., Lowenstam, H., and Urey, H. C. (1951). Carbonate-Water Isotopic Temperature Scale. *GSA Bulletin*, 62(4):417–426.

Goswami, B., Boers, N., Rheinwalt, A., Marwan, N., Heitzig, J., Breitenbach, S., and Kurths, J. (2018). Abrupt transitions in time series with uncertainties. *Nature Communications*, 9(48).

Kejriwal, M., Perron, P., and Zhou, J. (2013). Wald tests for detecting multiple structural changes in persistence. *Econometric Theory*, 29(2):289–323.

Kurozumi, E. and Tuvaandorj, P. (2011). Model selection criteria in multivariate models with multiple structural changes. *Journal of Econometrics*, 164(2):218–238.

Liu, J., Wu, S., and Zidek, J. V. (1997). On Segmented Multivariate Regressions. *Statistica Sinica*, 7:497–525.

Livina, V. N., Kwasniok, F., and Lenton, T. M. (2010). Potential analysis reveals changing number of climate states during the last 60 kyr. *Climate of the Past*, 6(1):77–82.

Marwan, N., Carmen Romano, M., Thiel, M., and Kurths, J. (2007). Recurrence plots for the analysis of complex systems. *Physics Reports*, 438(5):237–329.

Marwan, N., Donges, J. F., Donner, R. V., and Eroglu, D. (2021). Nonlinear time series analysis of palaeoclimate proxy records. *Quaternary Science Reviews*, 274:107245.

Nguyen, L., Yamamoto, Y., and Perron, P. (2023). *mbreaks: Estimation and Inference for Structural Breaks in Linear Regression Models*. R package version 1.0.0.

Reikard, G. (2021). Forecasting paleoclimatic data with time series models. *Results in Geophysical Sciences*, 6:100015.

Rousseau, D.-D., Bagniewski, W., and Lucarini, V. (2023). A Punctuated Equilibrium Analysis of the Climate Evolution of Cenozoic Exhibits a Hierarchy of Abrupt Transitions. *Scientific Reports*, 13:11290.

Shackleton, N. (1967). Oxygen Isotope Analyses and Pleistocene Temperatures Re-assessed. *Nature*, 215:15–17.

Tierney, J. E., Poulsen, C. J., Montañez, I. P., Bhattacharya, T., Feng, R., Ford, H. L., Hönisch, B., Inglis, G. N., Petersen, S. V., Sagoo, N., Tabor, C. R., Thirumalai, K., Zhu, J., Burls, N. J.,

Foster, G. L., Goddérus, Y., Huber, B. T., Ivany, L. C., Turner, S. K., Lunt, D. J., McElwain, J. C., Mills, B. J. W., Otto-Bliesner, B. L., Ridgwell, A., and Zhang, Y. G. (2020). Past climates inform our future. *Science*, 370(6517):eaay3701.

Westerhold, T., Marwan, N., Drury, A. J., Liebrand, D., Agnini, C., Anagnostou, E., Barnet, J. S. K., Bohaty, S. M., Vleeschouwer, D. D., Florindo, F., Frederichs, T., Hodell, D. A., Holbourn, A. E., Kroon, D., Lauretano, V., Littler, K., Lourens, L. J., Lyle, M., Pälike, H., Röhl, U., Tian, J., Wilkens, R. H., Wilson, P. A., and Zachos, J. C. (2020). An astronomically dated record of Earth's climate and its predictability over the last 66 million years. *Science*, 369(6509):1383–1387.

Yao, Y.-C. (1988). Estimating the number of change-points via Schwarz' criterion. *Statistics & Probability Letters*, 6(3):181–189.

Zachos, J., MO, P., Sloan, L., Thomas, E., and Billups, K. (2001). Trends, Rhythms, and Aberrations in Global Climate 65 Ma to Present. *Science (New York, N.Y.)*, 292:686–93.

A Simulation study

A.1 Serially uncorrelated error term

In this appendix, we assess whether the methodology by Bai and Perron (1998, 2003) can be used to accurately estimate the number and timing of breakpoints in a state-wise non-stationary time series. We conduct 1000 simulations for each data-generating process (DGP) with a sample size of 500. All the DGPs considered have the following form,

$$\begin{aligned} y_t &= c_1 + \varphi_1 y_{t-1} + \varepsilon_t, \quad \varepsilon_t \stackrel{i.i.d.}{\sim} \mathcal{N}(0, \sigma^2) \quad \text{for } t \leq T/2 \\ y_t &= c_2 + \varphi_2 y_{t-1} + \varepsilon_t, \quad \varepsilon_t \stackrel{i.i.d.}{\sim} \mathcal{N}(0, \sigma^2) \quad \text{for } t > T/2. \end{aligned} \quad (8)$$

Hence, we consider a single breakpoint in the middle of the sample interval, namely at $t = 250$. We examine eight DGPs, each specified and described in Table 2.

The DGPs range from random walk models with a break in the drift term to models with breaks in both the intercept and the AR coefficient. For comparison, we include a random walk without breakpoints as the sixth model. For each of the DGPs, we are interested in the performance of the methodology by Bai and Perron (1998, 2003) in estimating the breakpoint and confidence intervals. The model specifications from Section 3.2 are applied, and we use the implementation outlined in Section 3.3. We use the R-package *mbreaks* by Nguyen et al. (2023), and we impose a single breakpoint in the estimation. The left and right panels of figures 5 through 12 display realisations of the DGP and density plots of the estimated breakpoints for each of the models, respectively.

DGP	σ	c_1	c_2	φ_1	φ_2	Description
1	1	0.1	0.2	1	1	Small break in the drift term of a RW
2	1	0.1	1	1	1	Large break in the drift term of a RW
3	1	0.1	1	0.95	0.95	Large break in the intercept and a fixed AR-coefficient
4	1	0.1	1	0.95	1	Break in the intercept and small break in the AR-coefficient
5	1	0.1	1	0.5	1	Break in the intercept and large break in the AR-coefficient
6	1	1	1	1	1	RW with a drift <i>without</i> a breakpoint
7	0.5	0.1	1	1	1	Large break in the drift of a RW with low variance
8	1	0.1	1	0.5	0.5	Large break in the intercept and a low fixed AR-coefficient

Table 2: Data-generating processes for the simulation study and short descriptions. RW: random walk.

The results are summarised in Table 3, which provides the mean of the estimated breakpoints, and medians of the lower and upper boundaries of the estimated 95% CIs are tabulated along with their coverage rates for each model and DGP.

DGP	Mean				Fixed AR				AR			
	BP est.	Lower	Upper	Coverage	BP est.	Lower	Upper	Coverage	BP est.	Lower	Upper	Coverage
1	301	174	655	57.1%	251	216	336	43.4%	290	240	316	22.7%
2	333	-386	332	95.4%	249	237	262	93%	249	236	256	77.2%
3	263	253	284	41.4%	256	239	260	89.9%	251	241	260	85.9%
4	340	-190	340	97.5%	249	239	260	95.8%	249	238	250	65.8%
5	340	-114	340	97.1%	250	239	258	97%	250	241	250	72.9%
6	249	-3325	3976	×	253	142	371	×	254	202	312	×
7	333	-282	330	92%	249	246	253	97.8%	249	246	253	96%
8	249	237	264	95.1%	248	236	263	95.2%	248	236	263	94.5%

Table 3: Mean of the estimated breakpoints and medians of the lower and upper boundary of the estimated confidence intervals, along with the coverage rates for each model specification and DGP. DGP 6 is simulated without a breakpoint, so the coverage rate is irrelevant and indicated by \times .

In the first DGP, a random walk with a small drift term break, we observe that the mean of the estimated breakpoints is later than the true breakpoint in all model specifications. Additionally, the density plots exhibit asymmetry around the true breakpoint. This is expected due to the low magnitude of the break in the drift term, which creates a subtle change in the overall stochastic trend, making accurate breakpoint detection difficult. In the second DGP with a larger drift term break, the estimated breakpoints exhibit a narrower and more bell-shaped density. The mean estimated breakpoints for the Fixed AR and AR models slightly precede the true breakpoint. However, the Mean model performs poorly, with the mean of the estimated breakpoints far from the true breakpoint.

In the third DGP, both the Fixed AR and AR models produce mean estimated breakpoints slightly later than the true breakpoint. The Mean model exhibits better performance in this DGP than in the second DGP. The fourth DGP has a break in the intercept and the AR-coefficient from

0.95 to 1, resulting in a state-wise non-stationary model. This change leads to breakpoint estimates very close to the true breakpoint, except in the Mean model. A similar outcome is observed in the fifth DGP, which features a larger increase in the AR-coefficient.

In the sixth DGP, which is defined without any breakpoints, the Mean model estimates breakpoints near the midpoint of the sample period, while the other two specifications yield inconclusive results. In the seventh DGP, the AR and Fixed AR models produce estimates close to the true breakpoint. However, the Mean model continues to produce breakpoint estimates far from the true value. Examining the eighth DGP, the three models perform almost equally well.

Overall, the Fixed AR and AR models tend to perform well in non-stationary scenarios, estimating breakpoints close to the true breakpoints. The methodology, however, appears to struggle with accurately estimating the true breakpoint in cases of minor changes between states and large error term variance. In contrast, the Mean model does not perform well in DGPs featuring gradual changes, aligning with theoretical expectations as detailed in Bai and Perron (2003).

The coverage rate of a CI is the proportion of times the CI covers the true breakpoint, here at $t = 250$. We find that the CIs of the Mean model are generally very wide and have varying coverage. In the Fixed AR and AR models, the CIs are typically narrower. The coverage rates are best in the DGPs with large differences between the states as seen in DGPs 4, 5, 7 and 8 using the Fixed AR model specification, which is in line with the findings of Bai and Perron (2003). For the AR model, the coverage rates are only close to the desired 95% in the seventh and eighth DGP, indicating that the CIs are inadequate in most of the DGPs considered.

DGP	Mean			Fixed AR			AR		
	BIC	LWZ	KT	BIC	LWZ	KT	BIC	LWZ	KT
1	3.0 (0%)	3.0 (0%)	3.0 (0%)	0.2 (15%)	0.0 (0%)	3.0 (0%)	0.1 (6%)	0.0 (0%)	0.0 (3%)
2	3.0 (0%)	3.0 (0%)	3.0 (0%)	1.0 (97%)	0.8 (82%)	3.0 (0%)	1.0 (94%)	0.5 (46%)	1.0 (93%)
3	2.9 (0%)	2.7 (4%)	3.0 (0%)	1.0 (94%)	0.2 (16%)	2.9 (0%)	0.9 (85%)	0.0 (0%)	0.7 (70%)
4	3.0 (0%)	3.0 (0%)	3.0 (0%)	1.0 (98%)	1.0 (98%)	2.8 (0%)	1.0 (99%)	0.9 (92%)	1.0 (99%)
5	3.0 (0%)	3.0 (0%)	3.0 (0%)	1.0 (99%)	1.0 (97%)	2.7 (0%)	1.0 (99%)	1.0 (100%)	1.0 (99%)
6	3.0 (0%)	3.0 (0%)	3.0 (0%)	0.0 (98%)	0.0 (100%)	3.0 (0%)	0.0 (100%)	0.0 (100%)	0.0 (100%)
7	3.0 (0%)	3.0 (0%)	3.0 (0%)	1.0 (99%)	1.0 (100%)	3.0 (0%)	1.0 (98%)	1.0 (100%)	1.0 (98%)
8	1.5 (63%)	1.0 (98%)	1.3 (72%)	1.0 (99%)	1.0 (100%)	1.3 (73%)	1.0 (100%)	1.0 (98%)	1.0 (100%)

Table 4: Means of the estimated number of breakpoints for each model specification across different DGPs, rounded to one decimal. Percentages indicate the proportion of estimates equal to the true number of breakpoints.

Table 4 shows the mean number of breakpoints estimated for each DGP and method, along with the proportion of correctly estimated breakpoints. The difficulty in accurately estimating gradual changes using the Mean model is also evident when estimating the number of breakpoints.

This model specification leads to overestimating the number of breakpoints in all DGPs considered except DGP 8, where it performs well. The BIC criterion in the Fixed AR specification performs very well, with an estimated number of breakpoints equal to the true number in most simulations in DGP 2-8. The LWZ criterion performs almost equally well except in the third DGP, while the KT criterion vastly overestimates the number of breakpoints in DGP 1-7. In the AR model, the information criteria all perform well in DGPs 2-8 except for the third DGP where the LWZ criterion underestimates the number of breakpoints.

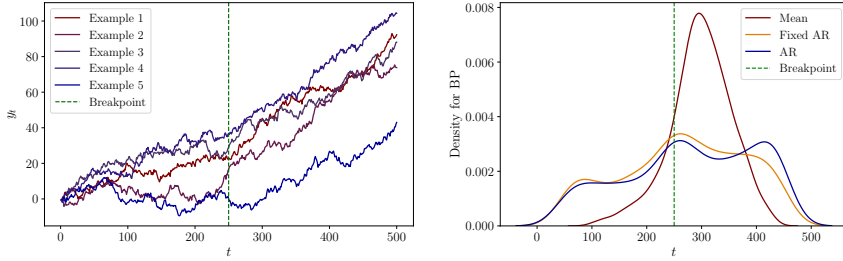


Figure 5: DGP 1: Left: Five process realisations. Right: The densities of the estimated breakpoints for each specification.

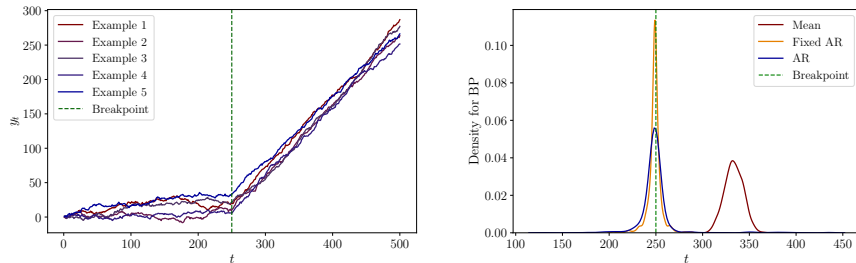


Figure 6: DGP 2: Left: Five process realisations. Right: The densities of the estimated breakpoints for each specification.

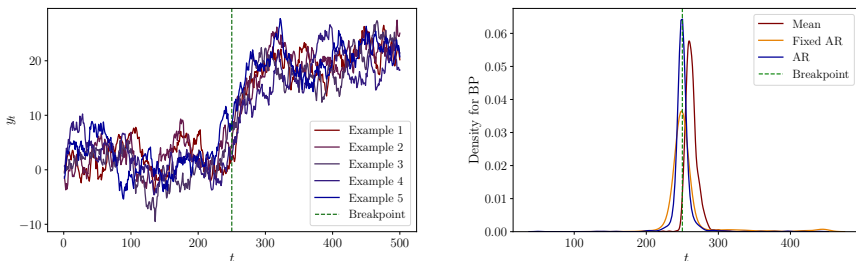


Figure 7: DGP 3: Left: Five process realisations. Right: The densities of the estimated breakpoints for each specification.

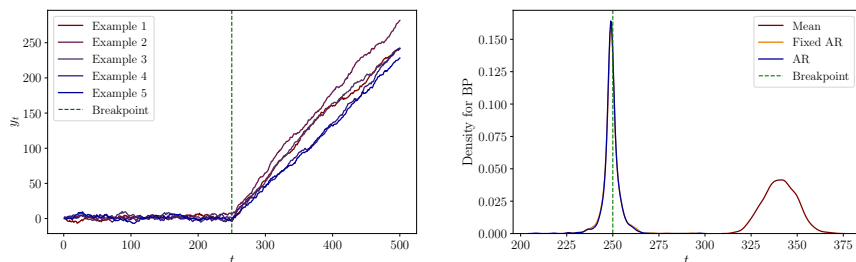


Figure 8: DGP 4: Left: Five process realisations. Right: The densities of the estimated breakpoints for each specification.

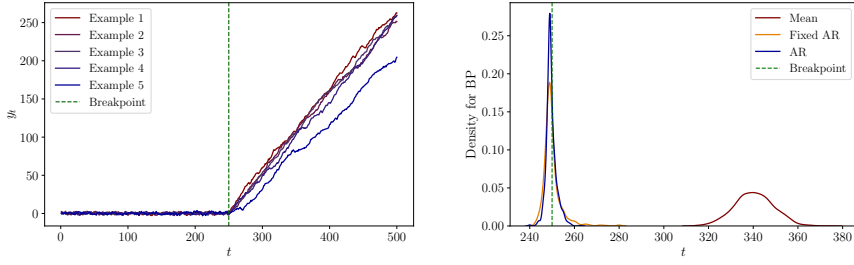


Figure 9: DGP 5: Left: Five process realisations. Right: The densities of the estimated breakpoints for each specification.

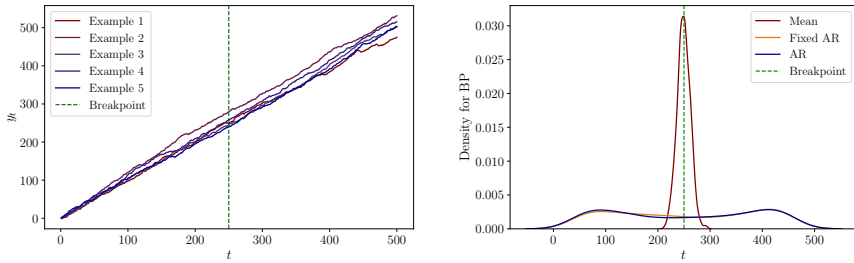


Figure 10: DGP 6: Left: Five process realisations. Right: The densities of the estimated breakpoints for each specification.

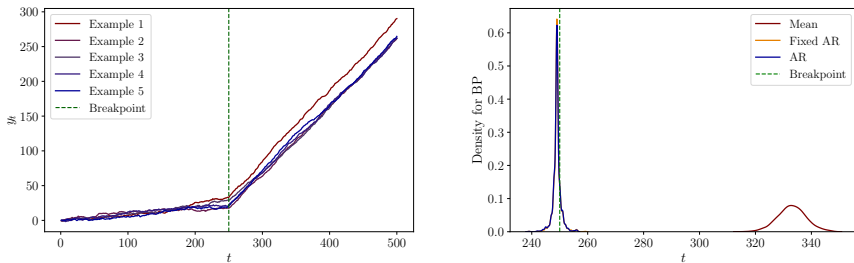


Figure 11: DGP 7: Left: Five process realisations. Right: The densities of the estimated breakpoints for each specification.

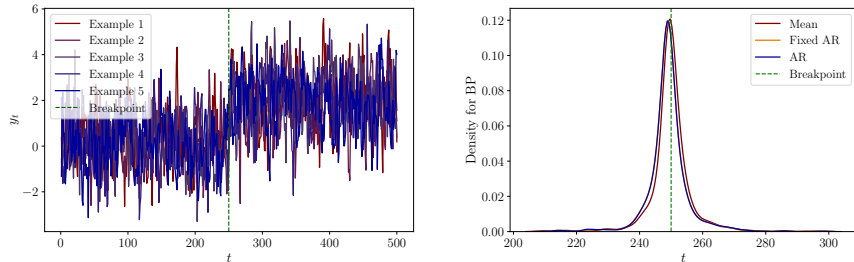


Figure 12: DGP 8: Left: Five process realisations. Right: The densities of the estimated breakpoints for each specification.

A.2 Serially correlated error term

A possible extension of the simulation study outlined in Equation (8) is allowing the error term to exhibit serial correlation. We use the same DGPs as before, but generate $\{\varepsilon_t\}_{t=1}^T$ as follows,

$$\varepsilon_t = \psi \varepsilon_{t-1} + \theta \eta_{t-1} + \eta_t, \quad \eta_t \stackrel{i.i.d.}{\sim} \mathcal{N}(0, \sigma_\eta^2) \quad \forall t. \quad (9)$$

We conduct 1000 simulations for each, with a sample size of 500. Here, we consider DGPs 2, 3, 4, 5, 7, and 8 as outlined in Table 2 and refer to these DGPs in the serially correlated cases as models 2_s , 3_s , 4_s , 5_s , 7_s , and 8_s . We set $\psi = \theta = 0.5$ and the standard deviation σ_η , such that the standard deviation of ε_t corresponds to the σ in Table 2. This is accomplished as follows,

$$\begin{aligned}\text{Var}(\varepsilon_t) &= \text{Var}(\psi\varepsilon_{t-1} + \theta\eta_{t-1} + \eta_t) \\ &= \psi^2 \text{Var}(\varepsilon_{t-1}) + \theta^2 \text{Var}(\eta_{t-1}) + 2\psi\theta \text{Cov}(\varepsilon_{t-1}, \eta_{t-1}) + \text{Var}(\eta_t) \\ &= \psi^2 \text{Var}(\varepsilon_{t-1}) + \theta^2 \sigma_\eta^2 + 2\psi\theta\sigma_\eta^2 + \sigma_\eta^2,\end{aligned}$$

since ε_{t-1} and η_{t-1} have zero means and $\mathbb{E}[\varepsilon_t\eta_t] = \phi\mathbb{E}[\varepsilon_{t-1}\eta_t] + \theta\mathbb{E}[\eta_t\eta_{t-1}] + \mathbb{E}[\eta_t^2] = \sigma_\eta^2$. Given stationarity of the process, which implies $\sigma^2 = \text{Var}(\varepsilon_t)$ for all t , we derive,

$$\sigma_\eta^2 = \sigma^2 \frac{1 - \psi^2}{1 + \theta^2 + 2\psi\theta}.$$

This adjustment ensures the comparability of the results between the two error term types.

In Figures 13 through 18, we plot examples of realisations and frequency plots of the estimated breakpoints using each of the models while imposing a single breakpoint in the estimation. The results are summarised in Table 5, which provides means of the estimated breakpoints and medians of the lower and upper boundary of the estimated confidence intervals, along with the coverage rates for each model specification and DGP. Generally speaking, the mean of the estimated breakpoints are further from the true breakpoint and the CIs become wider compared to the results from the corresponding DGPs without serial correlation. It is evident that serial correlation in the error term makes it more difficult to estimate the dating of breaks. We find that the Fixed AR and AR models perform well for DGPs 7_s , which has a large difference between the states and low variance. This is in line with the theoretical framework by Bai and Perron (2003), who note that the estimated break dates are consistent even in the presence of serial correlation. The Fixed AR model performs well in DGPs 2_s , 4_s and 5_s where the mean of the estimated breakpoints is close to the true breakpoint, and confidence intervals are reasonably wide with acceptable coverage rates. The results of the AR model are less conclusive.

For the Mean and Fixed AR models, the coverage rates are generally close to the desired 95% and even higher in some DGPs. However, the CIs are also extremely wide, reaching outside the sample window in many DGPs. The CIs seem reasonable in the Fixed AR model for DGPs 2_s , 4_s , 5_s , and 7_s , where the coverage rates are close to 95% and the medians of the lower and upper bounds of the CIs are not too extreme. The CIs for the AR model are generally wider than in the version without serial correlation in the error term. In the AR model, the coverage rates are lower than the desired 95%, but it seems that DGPs with large breaks have higher coverage

rates. The relatively poor performance is in line with the theoretical framework by Bai and Perron (2003). The authors note that the construction of the CIs rely on having no serial correlation in the error term if a lagged dependent variable is included as a regressor, which has coefficients that are subject to breakpoints.

DGP	Mean				Fixed AR				AR			
	BP est.	Lower	Upper	Coverage	BP est.	Lower	Upper	Coverage	BP est.	Lower	Upper	Coverage
	2 _s	332	-1400	335	95.9%	247	188	312	95.7%	261	190	299
3 _s	266	60	787	90.6%	285	-112	656	97.2%	276	156	421	77.1%
4 _s	340	-776	339	94.9%	252	197	301	96.9%	264	195	277	84.9%
5 _s	342	-329	340	96.2%	256	196	266	96.4%	259	192	250	70.8%
7 _s	333	-1708	329	92.3%	249	230	270	97.6%	251	230	267	92.8%
8 _s	250	122	370	98.3%	245	-5	492	99.8%	247	23	490	97.4%

Table 5: Mean of the estimated breakpoints and medians of the lower and upper boundary of the estimated confidence intervals, along with the coverage rates for each model specification and DGP.

Table 6 shows the mean number of breakpoints estimated for each DGP and method, along with the proportion of correctly estimated number. In the Mean model, all information criteria overestimate the number of breakpoints. An important exception is the eighth DGP, where the performance is better, as in the case without serial correlation. In the Fixed AR and AR model specifications, the LWZ criterion generally performs well, while both the BIC and the KT criteria generally overestimate. However, the LWZ criterion leads to underestimating the number of breakpoints in DGPs 3_s and 8_s. These two DGPs are characterised by fixed AR-coefficients that are lower than one. This implies that these two processes do not exhibit an autoregressive unit root. Hence, it seems that the LWZ criterion performs well in cases of state-wise non-stationarity or switching between stationary and non-stationary states.

Compared to the findings in the DGPs without serial correlation, it is clear that the proportion of correct estimates are lower for most DGPs and model specifications. Overall, the best performing criterion seems to be the LWZ criterion in the Fixed AR and AR models, while the Mean model typically leads to overestimating the number of breakpoints.

DGP	Mean			Fixed AR			AR		
	BIC	LWZ	KT	BIC	LWZ	KT	BIC	LWZ	KT
2 _s	3.0 (0%)	3.0 (0%)	3.0 (0%)	1.9 (32%)	0.9 (70%)	2.9 (0%)	1.8 (37%)	0.7 (61%)	1.9 (33%)
3 _s	3.0 (0%)	2.8 (2%)	3.0 (0%)	0.7 (33%)	0.0 (0%)	2.7 (3%)	0.3 (19%)	0.0 (0%)	0.4 (17%)
4 _s	3.0 (0%)	3.0 (0%)	3.0 (0%)	1.7 (45%)	1.0 (85%)	2.8 (1%)	1.6 (51%)	0.8 (79%)	1.6 (47%)
5 _s	3.0 (0%)	3.0 (0%)	3.0 (0%)	1.8 (5%)	1.1 (85%)	2.8 (0%)	1.7 (40%)	1.0 (92%)	1.6 (49%)
7 _s	3.0 (0%)	3.0 (0%)	3.0 (0%)	1.9 (34%)	1.1 (89%)	3.0 (0%)	1.9 (34%)	1.0 (96%)	1.9 (32%)
8 _s	2.2 (21%)	1.2 (78%)	2.2 (23%)	0.4 (35%)	0.0 (0%)	1.9 (36%)	0.0 (4%)	0.0 (0%)	0.0 (3%)

Table 6: Means of the estimated number of breakpoints for each model specification across different DGPs, rounded to one decimal. Percentages indicate the proportion of estimates equal to the true number of breakpoints.

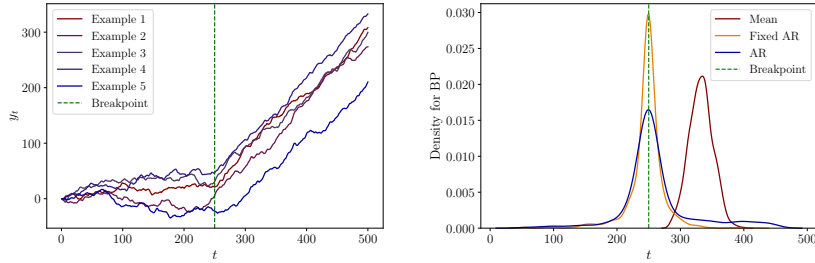


Figure 13: DGP 2_s: Left: Five process realisations. Right: The densities of the estimated breakpoints for each specification.

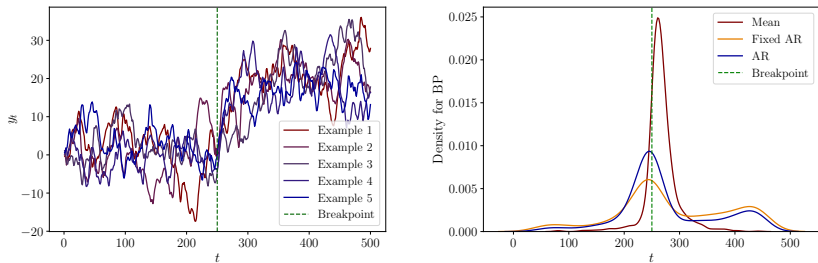


Figure 14: DGP 3_s: Left: Five process realisations. Right: The densities of the estimated breakpoints for each specification.

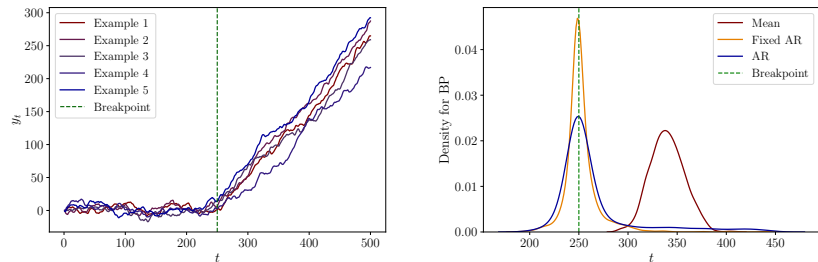


Figure 15: DGP 4_s: Left: Five process realisations. Right: The densities of the estimated breakpoints for each specification.

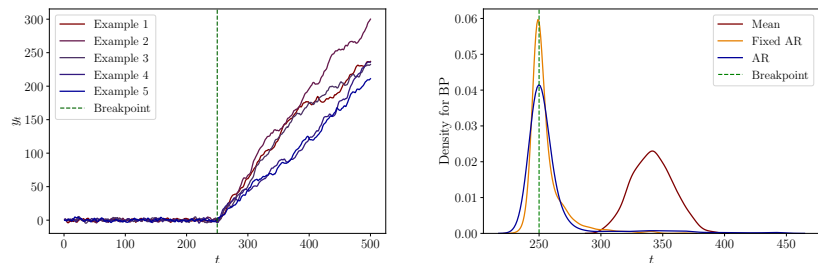


Figure 16: DGP 5_s: Left: Five process realisations. Right: The densities of the estimated breakpoints for each specification.

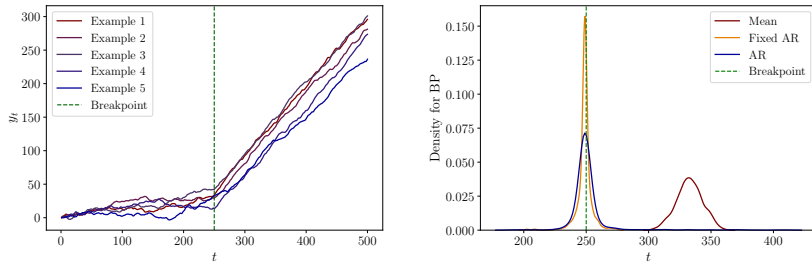


Figure 17: DGP 7_s: Left: Five process realisations. Right: The densities of the estimated breakpoints for each specification.

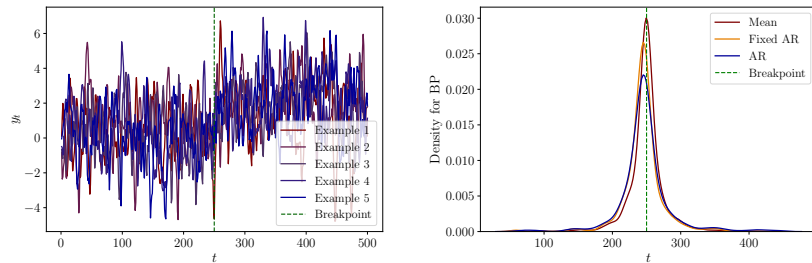


Figure 18: DGP 8_s: Left: Five process realisations. Right: The densities of the estimated breakpoints for each specification.

B Graphs

B.1 Reversed time

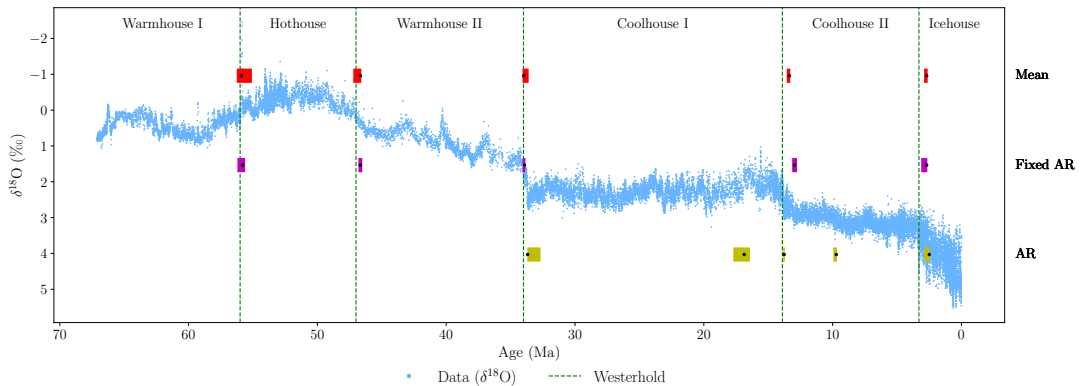


Figure 19: A comparison of estimated breakpoints using the Mean, Fixed AR, and AR model specifications for five breakpoints on 25 kyr binned data where the time frame is reversed. The black dots represent estimated breakpoints, while coloured shaded rectangles indicate 95% confidence intervals. The results overlay the $\delta^{18}\text{O}$ data from Westerhold et al. (2020) and their climate states.

B.2 One to fifteen breakpoints: Mean model

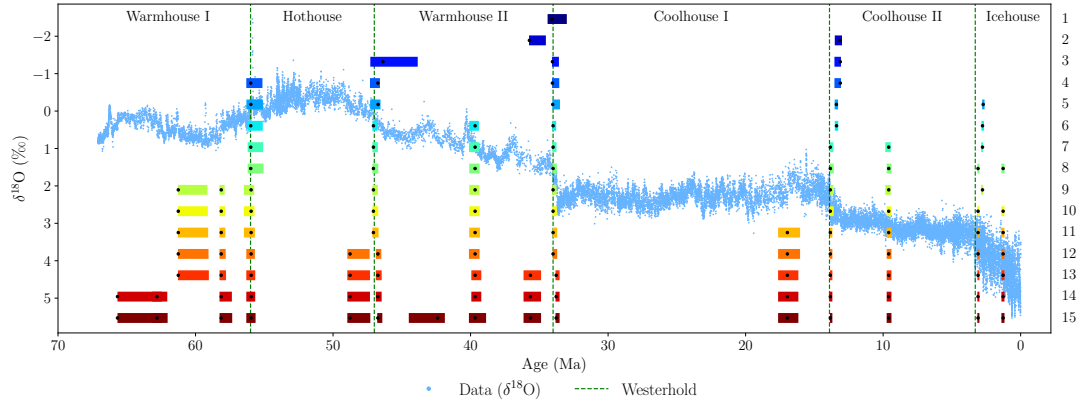


Figure 20: A comparison of estimated breakpoints using the Mean model for one to fifteen breakpoints on 25 kyr binned data. The minimum state length is set to $h = 1$ Myr. The black dots represent estimated breakpoints, while coloured shaded rectangles indicate 95% confidence intervals. The results overlay the $\delta^{18}\text{O}$ data from Westerhold et al. (2020) and their climate states.

B.3 One to fifteen breakpoints: AR model

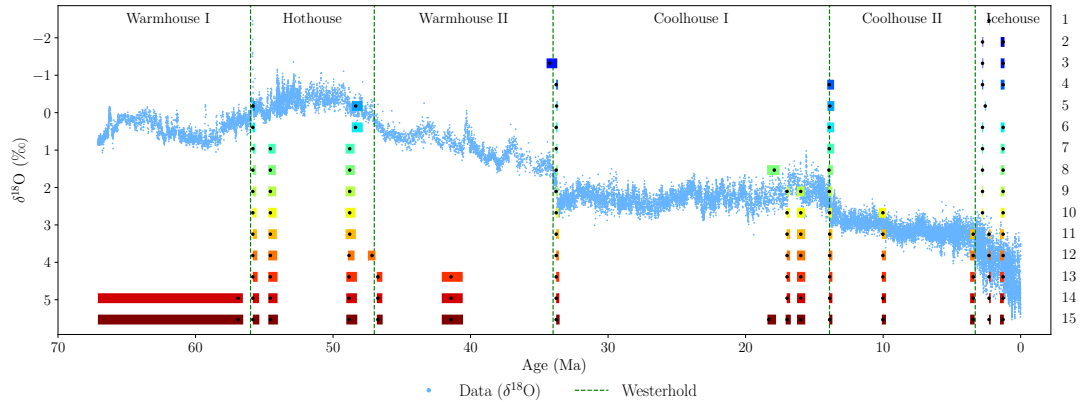


Figure 21: A comparison of estimated breakpoints using the AR model for one to fifteen breakpoints on 25 kyr binned data. The minimum state length is set to $h = 1$ Myr. The black dots represent estimated breakpoints, while coloured shaded rectangles indicate 95% confidence intervals. The results overlay the $\delta^{18}\text{O}$ data from Westerhold et al. (2020) and their climate states.

C Tables

C.1 Summary statistics: State-wise and full sample

Bin size	State	Mean	Sd.	Max.	Min.	Data points
5	Icehouse	4.037	0.463	5.405	3.05	660
5	Coolhouse II	3.072	0.237	4.172	1.885	2120
5	Coolhouse I	2.239	0.233	2.991	1.266	4020
5	Warmhouse II	0.897	0.366	1.894	-0.254	2600
5	Hothouse	-0.269	0.261	0.391	-2.014	1800
5	Warmhouse I	0.417	0.249	1.07	-0.215	2221
5	Full sample period	1.561	1.277	5.405	-2.014	13421
10	Icehouse	4.034	0.447	5.33	3.181	330
10	Coolhouse II	3.072	0.228	4.122	1.975	1060
10	Coolhouse I	2.239	0.221	2.877	1.324	2010
10	Warmhouse II	0.897	0.366	1.777	-0.254	1300
10	Hothouse	-0.269	0.256	0.308	-2.014	900
10	Warmhouse I	0.417	0.245	0.977	-0.12	1111
10	Full sample period	1.561	1.276	5.33	-2.014	6711
25	Icehouse	4.033	0.401	5.158	3.258	132
25	Coolhouse II	3.073	0.213	3.793	2.087	424
25	Coolhouse I	2.239	0.202	2.749	1.391	804
25	Warmhouse II	0.898	0.358	1.688	0.01	520
25	Hothouse	-0.269	0.245	0.218	-1.871	360
25	Warmhouse I	0.418	0.237	0.912	-0.065	445
25	Full sample period	1.561	1.273	5.158	-1.871	2685
50	Icehouse	4.042	0.359	4.757	3.264	66
50	Coolhouse II	3.072	0.206	3.72	2.156	212
50	Coolhouse I	2.24	0.188	2.713	1.567	402
50	Warmhouse II	0.898	0.354	1.656	0.182	260
50	Hothouse	-0.268	0.233	0.197	-1.871	180
50	Warmhouse I	0.419	0.233	0.867	-0.042	223
50	Full sample period	1.562	1.271	4.757	-1.871	1343
75	Icehouse	4.041	0.351	4.753	3.283	44
75	Coolhouse II	3.068	0.214	3.652	2.072	142
75	Coolhouse I	2.239	0.181	2.717	1.691	268
75	Warmhouse II	0.894	0.351	1.553	0.156	173
75	Hothouse	-0.26	0.203	0.167	-0.985	120
75	Warmhouse I	0.42	0.229	0.837	0.006	148
75	Full sample period	1.563	1.268	4.753	-0.985	895
100	Icehouse	4.047	0.344	4.673	3.4	33
100	Coolhouse II	3.073	0.201	3.625	2.353	106
100	Coolhouse I	2.241	0.175	2.685	1.739	201
100	Warmhouse II	0.898	0.349	1.601	0.228	130
100	Hothouse	-0.263	0.203	0.155	-0.985	90
100	Warmhouse I	0.42	0.229	0.832	0.007	112
100	Full sample period	1.562	1.269	4.673	-0.985	672
Without binning	Icehouse	4.064	0.533	5.53	2.66	3731
Without binning	Coolhouse II	3.102	0.254	4.49	1.84	6282
Without binning	Coolhouse I	2.251	0.242	3.263	1.026	6669
Without binning	Warmhouse II	0.916	0.357	1.894	-0.254	1786
Without binning	Hothouse	-0.279	0.255	0.391	-2.46	3030
Without binning	Warmhouse I	0.428	0.25	1.07	-0.215	2761
Without binning	Full sample period	2.128	1.445	5.53	-2.46	24259

Table 7: Summary statistics of the binned data with bin sizes (5, 10, 25, 50, 75, and 100 kyr) and the $\delta^{18}\text{O}$ data without binning for each of the states identified by Westerhold et al. (2020) and the full sample period.

C.2 Estimated breakpoints: 5 breakpoints

Bin size	BP index	Mean		Fixed AR		AR	
		Estimate	95% CI	Estimate	95% CI	Estimate	95% CI
5	1	55.96	(56.08, 55.88)	56	(56.08, 55.92)	33.74	(33.74, 33.72)
5	2	46.72	(46.84, 46.68)	46.73	(46.76, 46.68)	16.96	(17.36, 16.78)
5	3	34.02	(34.02, 33.92)	34.05	(34.08, 34.02)	13.82	(13.84, 13.78)
5	4	13.36	(13.4, 13.32)	13.41	(13.46, 13.34)	9.56	(9.59, 9.51)
5	5	2.74	(2.84, 2.72)	2.74	(3.1, 2.72)	3.36	(3.82, 3.36)
10	1	55.97	(56.15, 55.79)	55.99	(56.15, 55.88)	33.77	(33.77, 33.72)
10	2	46.73	(46.84, 46.64)	46.73	(46.77, 46.64)	17.88	(18.32, 17.64)
10	3	34.02	(34.03, 33.9)	34.15	(34.18, 34.09)	13.82	(13.84, 13.75)
10	4	13.36	(13.4, 13.3)	13.82	(13.89, 13.72)	9.59	(9.72, 9.45)
10	5	2.73	(2.81, 2.7)	2.74	(3.18, 2.71)	2.74	(2.88, 2.72)
25	1	55.98	(56.3, 55.1)	56.02	(56.58, 55.7)	55.82	(55.85, 55.68)
25	2	46.72	(47.3, 46.55)	46.72	(46.82, 46.45)	48.35	(48.62, 47.85)
25	3	34.02	(34.05, 33.5)	34.15	(34.22, 34.0)	33.75	(33.75, 33.67)
25	4	13.4	(13.52, 13.28)	13.88	(13.98, 13.65)	13.88	(14.05, 13.55)
25	5	2.72	(2.8, 2.62)	2.78	(3.08, 2.7)	2.58	(2.6, 2.55)
50	1	55.95	(56.2, 54.6)	56	(57.1, 55.35)	56	(56.65, 55.7)
50	2	46.7	(48.15, 46.45)	47.1	(47.25, 46.55)	48.8	(49.1, 40.45)
50	3	34.05	(34.05, 32.8)	34.2	(34.3, 33.9)	33.75	(33.75, 33.6)
50	4	13.8	(14.15, 13.6)	13.85	(14.0, 13.45)	16.95	(17.35, 16.7)
50	5	2.75	(2.9, 2.5)	3.15	(3.4, 3.0)	14.3	(14.55, 12.8)
75	1	55.95	(56.32, 53.78)	56.25	(57.45, 54.75)	55.95	(56.32, 55.5)
75	2	46.72	(50.62, 46.42)	47.1	(47.48, 46.42)	53.32	(53.62, 50.1)
75	3	34.05	(34.05, 30.9)	34.2	(34.42, 33.67)	34.05	(34.05, 33.83)
75	4	13.35	(13.8, 12.98)	13.88	(14.1, 13.12)	16.95	(17.32, 16.5)
75	5	2.78	(3.38, 2.4)	3.15	(3.52, 2.92)	14.48	(15.08, 14.25)
100	1	56	(56.4, 54.0)	56.2	(57.7, 54.5)	56	(56.3, 55.5)
100	2	46.7	(52.5, 46.3)	47.1	(47.7, 46.3)	53.4	(53.8, 52.1)
100	3	34.1	(34.1, 29.4)	34.2	(34.5, 33.4)	49.1	(50.8, 48.8)
100	4	13.8	(14.7, 13.4)	13.9	(14.1, 12.9)	34.1	(34.1, 33.8)
100	5	2.9	(4.2, 2.3)	3.4	(3.8, 3.2)	13.8	(15.7, 12.9)

Table 8: Estimated breakpoints and their 95% confidence intervals (in Ma) where the number of breakpoints is fixed to 5, and all values are rounded to two decimals. The table shows estimates for each method across bin sizes 5, 10, 25, 50, 75, and 100 kyr.